Trans Indian Inst Met (2019) 72(2):369–381
https://doi.org/10.1007/s12666-018-1488-4

TECHNICAL PAPER

Development of Speciality Grade Wire by Controlling the Inclusions in High-Carbon Steel Using Synthetic Slag Treatment

G. K. Mandal[1] · Ashok Kamaraj[1] · M. M. Humane[1] · R. K. Minj[1] · S. K. Das[1] · R. B. V. Ramana[2] · T. Venugopalan[2,3]

Received: 21 February 2018 / Accepted: 5 November 2018 / Published online: 6 December 2018

Abstract The high-carbon wire rods essentially permit controlled traces of the aluminium and calcium dissolved in the molten steel bath due to the generation of un-deformable complex oxide inclusions. These inclusions can be controlled by treating the liquid steel with suitable synthetic slag. In the present investigation, slag with suitable composition was synthetically prepared based on the thermodynamic study. After melting the plant wire rods, synthetic slag was added in the bath and slag–metal reactions were carried out at around 1600 °C for a pre-specified period. Experimental results showed significant improvement in inclusion rating of hot-rolled specimens prepared by induction melting for the residence time of about 30 min across the slag–metal reaction. It thus depicts that slag–metal reaction residence time of 15 min is rather less than the residence time of 30 min for any significant improvement in inclusion rating under identical reactions across the slag–metal interface.

Keywords High-carbon wire rod · Oxide inclusions · Synthetic slag · Thermodynamic study

✉ Ashok Kamaraj
srhsbioboy@yahoo.co.in

[1] CSIR-National Metallurgical Laboratory (NML), Jamshedpur, India

[2] Tata Steel Ltd, Jamshedpur, India

[3] Indian Institute of Technology (IIT) Madras, Chennai, India

1 Introduction

Non-metallic inclusions are generally originated during liquid steel processing, and they are difficult to remove completely from liquid steel. Presence of complex non-metallic inclusions in steels has become a major concern for the production of high-quality extra clean steels. Such inclusions are responsible for degrading both the mechanical property of steels and process interruptions in steel plants, resulting in huge productivity loss [1–3]. The mechanical properties of steel largely depend on the volume fraction, size, distribution, composition and morphology of the inclusions and precipitates [2–8]. During thermo-mechanical processing, the inclusions may deform and elongate or break into fragments along the rolling direction, as they have different mechanical properties compared with steel matrix. The plastic deformation of inclusions depends on chemical composition, which has a strong relationship with the melting point [9, 10]. Inclusions having high melting point and hardness, such as calcium aluminates and Al_2O_3, should be essentially non-deformable. Therefore, differential deformation behaviour of non-metallic inclusions and steel matrix during application of mechanical and thermal stresses results in catastrophic failures [4, 5]. Non-deformable complex inclusion is present in tier cord steel; however, it has major effect on the life of steel during its service.

Numerous investigations have been carried out in the past few decades focusing on both theoretical and experimental studies to control the inclusions in steel [11–18, 20]. Non-metallic inclusions in steel are generally classified as indigenous inclusions or exogenous inclusions according to their sources [1–3]. Indigenous inclusions are formed during the de-oxidation stage and during cooling and solidification of liquid steel. Exogenous inclusions are

mainly produced from slag entrapment, ladle glaze, erosion of refractories and steel re-oxidation. Non-metallic inclusions which are mainly present in wire rod steels are of $MnO–SiO_2–Al_2O_3–CaO–MnS$ types [1]. Critical control on the elements such as aluminium and calcium present in wire rod steel is essential to avoid non-deformable inclusions [21, 22]. The common non-deformable inclusions act as crack nucleating sites during thermo-mechanical processing of steel and are generally complex oxides of aluminium and calcium. It is therefore necessary to eliminate non-deformable inclusions by controlling the trace elements such as Al and Ca dissolved in the liquid steel bath. Complex de-oxidation of liquid steel with Si and Mn yields deformable inclusions having low melting point as de-oxidation products [19]. Even with the use of Mn and Si as complex deoxidizer, presence of aluminium in the liquid steel cannot totally be avoided for various other reasons.

Synthetic slag plays a major role in controlling the type of non-metallic inclusions in steel during liquid steel refining stages. It is reported that synthetic slag with basicity 1–1.2 avoids formation of non-deformable inclusions in the high-carbon wire rods [19, 21–23]. A specially designed synthetic slag in turn alters the chemistry and melting point of both inclusions and liquid steel and thus influences the metallurgical properties of the steel. The present investigators explored the scope of top slag treatment of high-carbon wire rod steels to modify the non-deformable inclusions to deformable, after ladle furnace treatment. This paper comprises of both theoretical and experimental investigations for evaluating plausible slag composition and ascertaining its efficacy with respect to controlling the inclusions in these high-carbon wire rods.

2 FactSage Investigation

Thermodynamic simulation software package FactSage has extensive applications on alloy design, slag–metal equilibrium studies and other high-temperature metallurgical process simulations. The thermodynamic properties and phase equilibria of the $CaO–Al_2O_3–SiO_2$ system have been assessed. The calculated pseudo-binary phase diagram for $CaO–SiO_2–Al_2O_3$ system keeping CaO/SiO_2 ratio equal to one is represented in Fig. 1. The binary phase diagram has been plotted using the phase diagram module available in FactSage. The figure shows that liquidus temperature of slag decreases with an increase in Al_2O_3 content in slag up to about 18% and thereafter it increases.

Thermodynamic calculations were also done by employing equilibrium modules and databases, namely FSSTEL, FactPS and FToxid to study the slag–metal reactions. Slag composition containing CaO/SiO_2 = 0.8–1.5, Al_2O_3 = 6–20% at 1600 °C was considered for slag–metal equilibrium study. The high-carbon wire rod supplied by steel plant was analysed for composition, and the same was considered for thermodynamic study. The results of addition of synthetic slag having composition 46%CaO, 46%SiO_2 and 8%Al_2O_3 in liquid steel after slag–metal reaction at equilibrium are shown in Fig. 2. The figure depicts the effect of amount of slag on equilibrium [Al] content in liquid steel and the final slag basicity. With

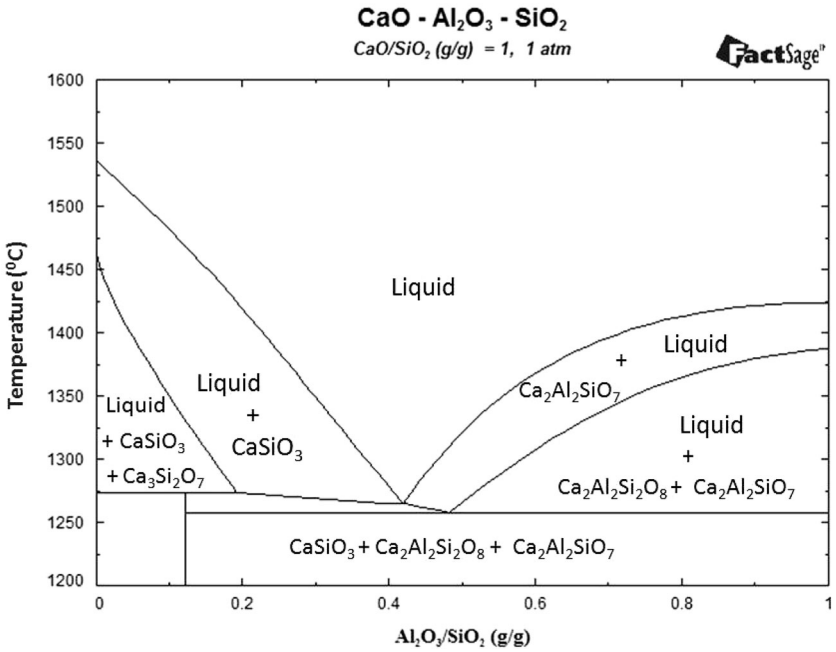

Fig. 1 Phase diagram of $CaO–Al_2O_3–SiO_2$ system

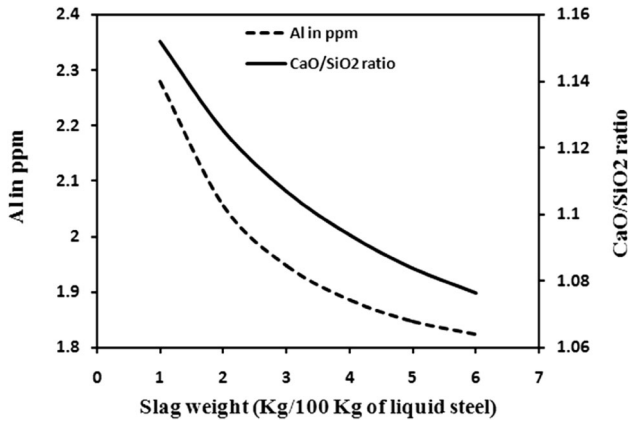

Fig. 2 Effect of slag (46%CaO, 46%SiO_2 and 8%Al_2O_3) weight on equilibrium [Al] content in liquid steel and final slag basicity

the increase in synthetic slag weight (1–6 wt% of liquid steel weight) added to liquid steel, equilibrium [Al] level in the liquid steel decreases. Prediction shows that equilibrium [Al] level in the bath decreases from 2.3 ppm to about 1.8 ppm with the increase in slag weight from 1 to 6 wt%. FactSage investigation also depicts that equilibrium final slag basicity decreases with the increase in slag weight, as shown in Fig. 1. Equilibrium calculation also predicts that final slag contains about 3.5 wt% MnO after slag–metal reaction.

Figure 3 reveals the effect of CaO/SiO_2 ratio and activity of Al_2O_3 on steel composition due to addition of 2 wt% synthetic slag having 8 wt% (Al_2O_3). The activity of Al_2O_3 in the synthetic slag increases from 0.001 to 0.007 while increasing the CaO/SiO_2 ratio from 0.8 to 1.5. With the same Al_2O_3 in the slag, high basicity of the synthetic slag during refining results in higher dissolved aluminium in molten steel. It is observed from Fig. 3a that slag with basicity < 1.2 reduces the aluminium in the liquid steel below 2.5 ppm. Therefore, thermodynamic calculation reveals that addition of suitable low-basicity synthetic slags in the wire rod steel bath can reduce Al level in the liquid steel in the range of 1–2 ppm or even below. It is also inferred from Fig. 3b that dissolved Al in the liquid steel increases beyond 2.5 ppm along with an decrease in dissolved oxygen from 18 ppm during addition of low-basicity synthetic slags. However, lower dissolved oxygen in the liquid steel expected to precipitate alumina or alumina-rich detrimental inclusions.

The dissolved aluminium level in the liquid steel bath will significantly be affected by the increase in Al_2O_3 content in the synthetic slag. The effect of wt% Al_2O_3 of the synthetic slag on steel composition can be thermodynamically corroborated using FactSage. Figure 4 depicts the effect of Al_2O_3 content of the slag on dissolved aluminium level of the bath due to addition of 2 wt% synthetic

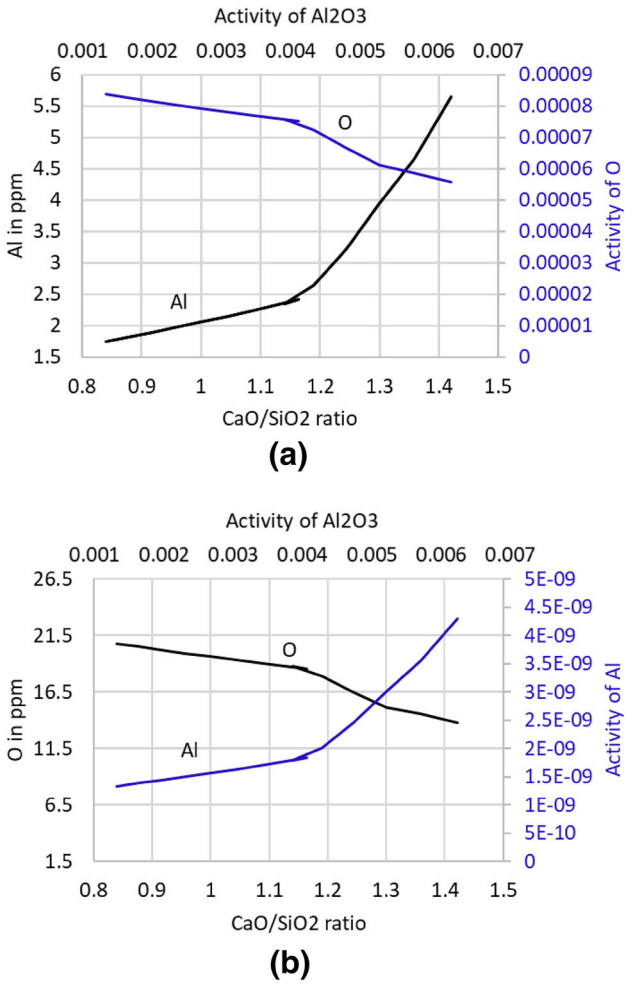

Fig. 3 Effect of CaO/SiO_2 ratio and activity of Al_2O_3 on **a** dissolved Al and activity of oxygen in liquid steel and **b** dissolved oxygen and activity of Al in liquid steel due to addition of 2 wt% synthetic slag keeping Al_2O_3 equal to 8 pct

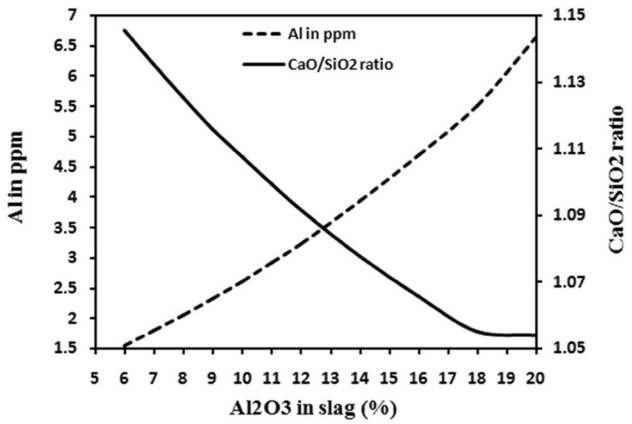

Fig. 4 Effect of (Al_2O_3) on steel composition due to addition of 2 wt% synthetic slag keeping CaO/SiO_2 ratio equal to one

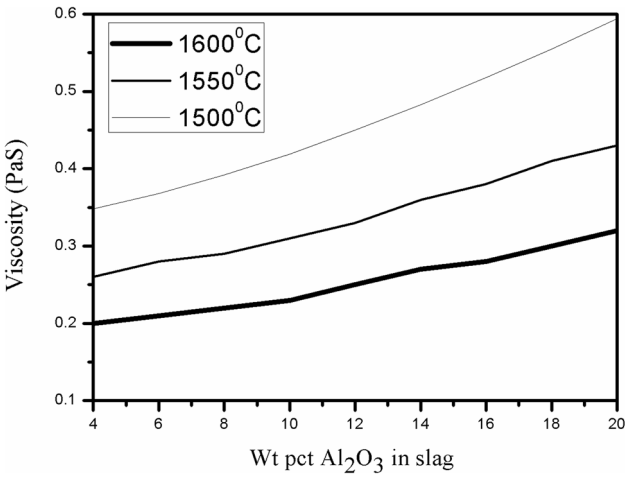

Fig. 5 Variation of viscosities with Al_2O_3 content of the CaO–Al_2O_3–SiO_2 system keeping CaO/SiO_2 ratio equal to one

slag keeping CaO/SiO_2 ratio equal to one. The change in dissolved [Al] level in liquid steel with (Al_2O_3) content in top slag is shown in the figure. There is a gradual increase in [Al] content in liquid steel with the increase in (Al_2O_3) content in slag. [Al] content in steel is in the range of 1.5 ppm to 6.5 ppm when (Al_2O_3) content in the slag is in the range of 6–20 wt%. Effect of (Al_2O_3) content in initial slag on final slag basicity is also analysed, and it is predicted that final slag basicity decreases with the increase in (Al_2O_3) content in initial slag.

Viscosity and melting point of slag determines the inclusion absorption ability of synthetic slag. Viscosity is seriously affected by the change in slag composition. Figure 5 represents the variation of viscosities (estimated by FactSage) of the slags with Al_2O_3 content of the CaO–Al_2O_3–SiO_2 system keeping CaO/SiO_2 ratio equal to one. In order to study the effect of temperature on the viscosity of the slag, the viscosities at 1600, 1550 and 1500 °C have also been included in the figure. As expected, the viscosity increases with decreasing temperature and increases gradually with increasing Al_2O_3 content of the slag. Therefore, Al_2O_3 content of the CaO–Al_2O_3–SiO_2 system needs to be controlled to maintain sufficient fluidity of the synthetic slag. Further, any solid phases, present in the synthetic slag at steelmaking temperature, should also be avoided to minimize the viscosity of liquid slag.

Based on the thermodynamic study, it can be concluded that synthetic slags having low basicity (CaO/SiO_2 = 0.9–1.2) and low Al_2O_3 content (max 10%) can control the harmful inclusions for the development of special grade high-carbon wires mainly for tire cord applications. The reaction between liquid steel and top slag having low basicity will help to produce very low level of dissolved aluminium and calcium in the molten steel bath. As a result, the liquid steel composition can be controlled by slag–metal reaction. Therefore, during solidification of liquid steel after slag–metal reaction, the generation of non-deformable calcium aluminates and Al_2O_3-type complex oxide inclusions can be avoided. It also helps in the generation of low-melting silicate-type oxide inclusions.

3 Experimental Investigation

The high-carbon wire rods of diameter around 5.5 mm supplied by the plant served as the starting material for the experiments in this study. Chemical compositions of these wire rods are given in Table 1. Based on the thermodynamic study, slag having low basicity (CaO/SiO_2 = 0.9–1.2) and low Al_2O_3 content (max 10%) was synthetically prepared in air induction furnace using graphite crucible. Graphite crucible was used for slag melting to avoid any other oxide contamination which could alter the slag composition. Laboratory grade extra pure silicon oxide (SiO_2), calcium oxide (CaO) and aluminium oxide (Al_2O_3) powders were mixed in desired proportion and charged into air induction furnace. After melting, slag was taken out of the furnace and air cooled. Cooled slags were further crushed into desired size for melting experiment using mortar and pestle. Composition of this slag prepared for the present investigation is given in Table 2.

Vacuum induction furnace of capacity 40 kg was used for melting and refining experiment. Initially, as-received wire rods were weighed for 35 kg and charged into the induction furnace. Temperature was slowly increased to melting point of charged material. After completion of melting and attaining temperature of about 1600 °C, composition of the liquid metal was checked with the help of lollypop sample taken from liquid steel bath. Thereafter, alloying elements were added to the bath to get desired steel composition to compensate the losses. After achieving the desired composition of liquid metal, synthetic slag was added to the bath for slag–metal reactions. Then, the steel bath was treated with mild vacuum to control the stirring of the bath for better slag–metal reactions. Slag–metal reactions continued for a pre-defined period (15 and 30 min) inside the furnace. Eventually, the liquid steel was tapped into a permanent mould inside the chamber. The ingot obtained from permanent mould was taken out of the chamber and allowed to cool in air. Slag samples from top of the ingot and attached to the furnace lining were collected and then sent for chemical analysis. X-ray powder diffraction (XRD) analysis was used with Cu Kα radiation in point focus for the phase identification of the slag samples. In all the experiments, 35 kg of materials was melted and 2 wt% synthetic slag was added and slag–metal reaction time was either 15 min or 30 min. Details of the experimental parameters are given in Table 3.

Table 1 Chemical composition of wire rods

Sample	C	Mn	S	P	Si	N	Cr
5.5 mm diameter	0.755	0.727	0.014	0.016	0.183	0.0062	0.131

Table 2 Composition of synthetic slags prepared for the present investigation

Composition (%)	CaO	SiO_2	Al_2O_3	CaO/SiO_2
	46.2	46.3	7.8	0.99

Table 3 Details of the experimental parameters for vacuum melting

Heat no.	Weight of wire rods (Kg)	Weight of synthetic slag (Kg)	Slag–metal reaction time (mins)
H-1	35	0.7	30
H-2	35	0.7	15

Ingots having the dimension of 100 mm × 100 mm cross section × ~ 500 mm length were sectioned to size of 100 mm × 100 mm × 50 mm and homogenized at 1150 °C for 4 h before forging. These hot-forged specimens of 25 mm thickness were hot rolled at 1100 °C to a final thickness of about 8 mm and were used for microstructural characterization.

Micro-structural characterization of all the un-etched specimens along the longitudinal direction was carried out by optical microscope (model: LEICA), scanning electron microscope (model: Hitachi S-3400N SEM) and energy-dispersive spectroscopy (Thermo NSS-6 EDS system) attached with SEM. Standard metallographic techniques were followed to prepare the specimens for characterization. For inclusion analysis, 12 random specimens from the same heat were prepared for optical microscopy and characterized at a magnification of 200 ×.

4 Results and Discussion

4.1 Chemical Analysis of Samples

Total oxygen and nitrogen content of the hot-rolled specimens obtained from induction melting along with 5.5-mm-diameter plant wire rod was analysed (using LECO analyser) and is given in Table 4. It is observed that total oxygen content of the specimens after slag–metal reactions of 15 and 30 min is about 47 and 25 ppm, respectively. This level of oxygen in steel is suitable for the production of wire rod steel [19]. Therefore, it is expected that cleanliness of steel, treated with synthetic slag at laboratory scale, has improved.

Table 4 Total oxygen and nitrogen content of the hot-rolled specimens obtained from induction melting along with 5.5-mm-diameter plant wire rod

Radicals	Total oxygen	Total nitrogen
5.5-mm-diameter wire rod	0.008	0.0052
H-1	0.0025	0.0052
H-2	0.0047	0.0039
Analytical tool/technique	Leco	Leco

Collected slag samples were also analysed by conventional analytical techniques to determine the chemical composition. Table 5 shows the composition of final slag. Collection of final slag after the slag–metal reactions from the induction furnace lining is not uniform due to the attachment of some refractory materials with the slag samples. Therefore, these slags always contain some higher percentage of MgO. This is also because of the monolithic MgO lining of experimental induction furnace. Analysis of final slag shows that MgO content is in the range of 25% for all the experiments irrespective of slag–metal reaction time.

Final slag analysis reveals that CaO/SiO_2 ratio is always less than one. The decrease in slag basicity is attributed to re-oxidation of Si and Mn before addition of synthetic slag due to atmospheric interaction. Oxide of SiO_2 and MnO forms slag phase and it alters the basicity of freshly added synthetic slag (~ 0.7). Further, alloying elements such as Fe–Si and Mn are added to maintain the desired composition of liquid steel and it does not encourage reduction of SiO_2 from slag, as the steel contains very less amount of aluminium. Therefore, slag–metal reactions start with top

Table 5 Analysis of final slag (wt%)

Slag	CaO	SiO_2	Al_2O_3	MnO	FeO	MgO	CaO/SiO_2
H-1	24	32.8	3.44	7.91	8.99	24.9	0.73
H-2	28.43	38.9	5.64	2	0.5	25.9	0.73

slag basicity less than unity. However, re-oxidation of liquid steel is unlikely to happen during industrial ladle furnace treatment as liquid steel is always protected from atmospheric contamination by top slag layer.

Analysis also shows that MnO content in final slag is about 8% for slag–metal reaction time of 30 min and it decreases to about 2% with the decrease in slag–metal reaction time of 15 min. Analysis of MnO in the final slag indicates the slag–metal reaction reaching towards equilibrium with the increase in experimental time after addition of synthetic slag in the liquid steel bath. It is well corroborating with the theoretical findings also. Isothermal thermodynamic calculation shows 3.5% MnO formation after slag–metal reaction. In experiments, it reaches up to 7.5% as the experimental time approaches 30 min. This may be due to some changes in thermodynamic equilibrium conditions as the heat is subjected to mild vacuum treatment after addition of synthetic slag.

XRD analysis of synthetic slag as well as final slags obtained after slag–metal reactions is shown in Fig. 6. The XRD spectra of the final slags obtained after 15 and 30 min of slag–metal reaction reveal the presence of peaks of several phases. These peaks are as expected for the above-mentioned composition of the final slags. It is interesting to note that X-ray diffraction reveals the presence of glassy phase for the synthetic slag prepared for the present investigation. It can therefore be concluded that no crystal is found during the preparation of synthetic slag.

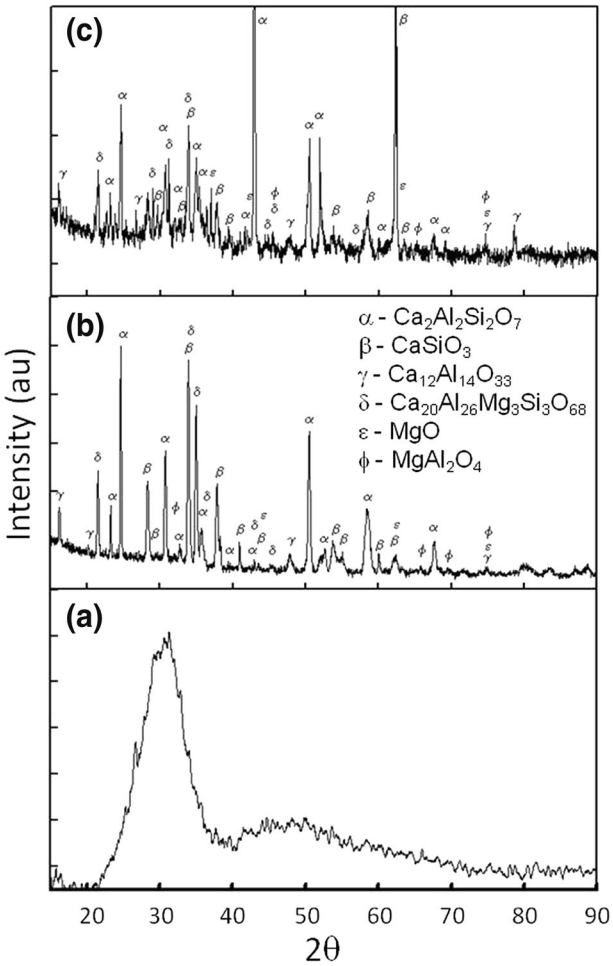

Fig. 6 XRD patterns of the slag samples, **a** synthetic slag, **b** final slag after 15 min of slag–metal reaction and **c** final slag after 30 min of slag–metal reaction

4.2 Characterization of Inclusions

4.2.1 Inclusions in as-Received 5.5-mm-Diameter Wire Rod (Sans Synthetic Slag)

Figure 7 depicts the optical micrographs of the inclusions of six hot-rolled specimens in 5.5-mm-diameter wire rod. These micrographs have been taken randomly from different positions of the wire rod in longitudinal section. These micrographs are obtained from worst field of each sample, i.e. the portion of each sample having maximum number of inclusions irrespective of their sizes. Micrographs clearly reveal the presence of many elongated, globular- and sharp corner-shaped inclusions. From these images, it is difficult to predict accurately the nature and chemical composition of the inclusions. However, these micrographs can give an idea about the nature of the inclusions based on the colour and shapes of the inclusions under optical micrographs along with their distribution.

Silicate inclusions are generally darker, elongated and continuous in nature and can be seen in many of these micrographs. Sulphide inclusions are generally grey coloured, elongated and not continuous like silicates. These breakable, elongated sulphide inclusions can also be seen in the micrographs. Both these silicate and sulphide inclusions are deformable in nature. Sometimes silicate inclusions are considered un-deformable in nature if length-to-thickness ratio of inclusions is less than three [19]. Alumina- and

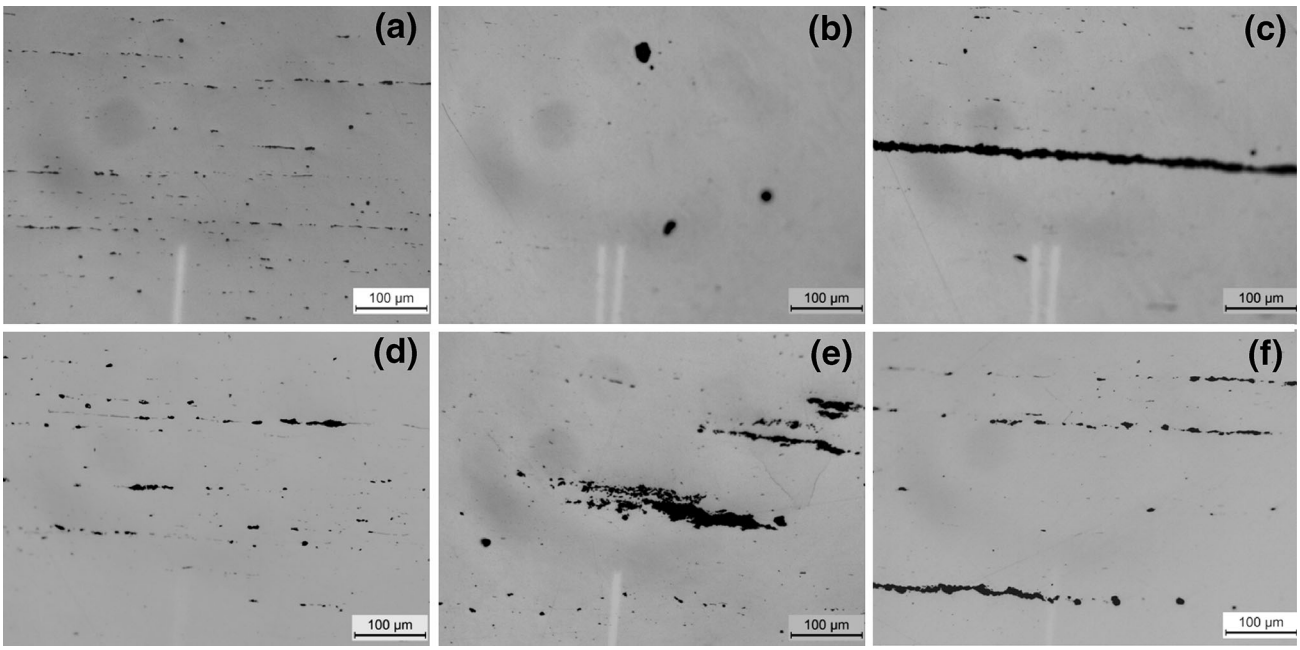

Fig. 7 Optical micrographs of inclusions in 5.5-mm-diameter wire rod

calcium-based complex oxides are generally globular, square or little elongated in shape based on the chemical composition of the inclusions. These inclusions are harmful and always non-deformable in nature. As these inclusions are harder than steel matrix, nucleation and growth of voids can take place at the interface between inclusion and matrix during wire drawing and lead to breakage. An inclusion is generally considered as un-deformable if aspect ratio (length-to-thickness ratio) is less than 3 [19].

Presence of many deformable and un-deformable inclusions is shown in Fig. 7. Figure 8 shows the SEM micrographs of the inclusions in 5.5-mm-diameter wire rod along with EDS analysis. Presence of continuous elongated inclusion is shown in Fig. 8a. Figure 8b shows the same inclusion at higher magnification. SEM micrograph at higher magnification clearly shows the presence of few globular- and almost square-shaped inclusions (dark phases) inside the elongated grey colour inclusion. SEM–EDS spot analysis has been conducted to determine the chemical compositions of the inclusions. Figure 8c and d depicts the EDS analysis of grey phase and black phase, respectively. EDS analysis conducted on grey phase indicates that the elongated continuous inclusion mainly consists of MnO–SiO_2-based oxide, whereas the dark phases reveal the peaks of aluminium, calcium, silicon and manganese. Therefore, it can be concluded that the dark phases inside the elongated inclusion mainly consist of CaO–Al_2O_3-based non-deformable complex oxides.

Morphology of various types of inclusions is shown in Fig. 9 along with EDS spot analysis taken from the inclusions. Figure 9a shows the morphology of MnS-type inclusions, which are always elongated and breakable in nature. MnS inclusion at higher magnification is shown in Fig. 9b. Presence of silica in aluminium- and calcium-based oxides makes the inclusions little elongated in nature as shown in Fig. 9c and d. Figure 9e shows the morphology of Al_2O_3-based phase showing the presence of sharp edges. CaO-based oxide inclusions are generally globular in shape as shown in Fig. 9f. Based on optical and SEM micrographs, it can be concluded that both sulphide and silicate inclusions are generally elongated and of deformable type. These are less harmful to mechanical properties of steel wires than the inclusions that are non-deformable in nature due to the presence of other oxides mainly Al_2O_3 and CaO. However, silicate inclusions are always present in the form of complex oxides and may be deformable- or non-deformable-type inclusions based on the presence of other oxides.

4.2.2 Inclusion in the Specimens Obtained from Heat-1 (with Synthetic Slag)

Figure 10 represents the optical micrographs of worst field of six specimens obtained from Heat-1. These hot-rolled specimens were prepared by melting the 5.5-mm-diameter wire rods with synthetic slag in a vacuum induction furnace for the residence time of about 30 min across the slag–metal reaction. Optical micrographs depict the significant improvement in steel cleanliness of hot-rolled specimens prepared by induction melting using synthetic slag treatment

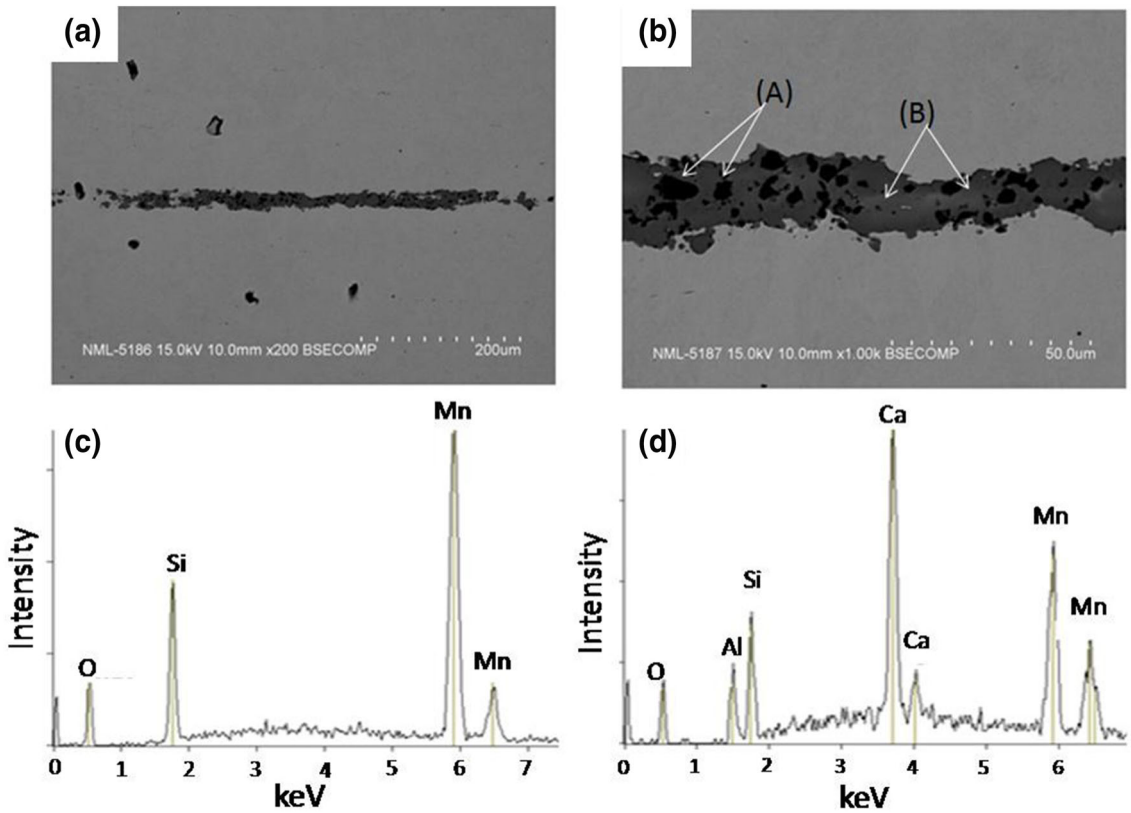

Fig. 8 SEM micrographs of the inclusions in 5.5-mm-diameter wire rod along with SEM–EDS analysis, **a** SEM image at lower magnification, **b** SEM image at higher magnification, **c** and **d** SEM–EDS analysis of black phases (A) and grey phases (B), respectively

in comparison with 5.5-mm-diameter of as-received wire rod. All the micrographs reveal less volume fraction of smaller-sized inclusions. Most of the specimens are almost free from harmful inclusions. Though, the presence of few smaller-sized globular inclusions can be seen.

SEM micrographs (Fig. 11) reveal the presence of mainly MnS inclusions in these specimens. SEM–EDS analysis shows that all these elongated and globular inclusions mainly consist of MnS particles. Presence of free oxide inclusions in these specimens is not observed by SEM–EDS analysis. However, few smaller-sized oxide particles are attached to some of the MnS inclusions as can be seen in higher-magnification SEM micrographs as shown in Fig. 11c and d. It is noted that the amount of deformation applied during hot rolling is not sufficient to make these small globular MnS particles elongated. SEM–EDS analysis shows that these globular inclusions are mainly deformable MnS type.

4.2.3 Inclusion in the Specimens Obtained from Heat-2 (with Synthetic Slag)

Figure 12 shows the optical micrographs of worst field of six hot-rolled specimens from Heat-2. These specimens were prepared by melting the 5.5-mm-diameter wire rods with synthetic slag in a vacuum induction furnace for the residence time of about 15 min across the slag–metal reaction. Optical micrographs depict that slag–metal reaction time of 15 min is not sufficient for much improvement in steel cleanliness in comparison with the identical reactions across the slag–metal interface with residence time of 30 min. Optical micrographs reveal the presence of both elongated and globular inclusions.

Figure 13 shows the selected SEM micrographs which reveals the presence of both elongated sulphide and oxide (both globular and irregular shaped) inclusions in these specimens. SEM micrographs confirm that MnS inclusions are always attached to oxides (Fig. 13a–d). Presence of free oxide at some of the location of the specimen is also observed. Figure 13e and f depicts the SEM micrographs of globular oxy-sulphide and oxide, respectively, as confirmed by EDS spot analysis. It is interesting to note that presence of these oxides is almost absent in the hot-rolled specimens obtained from Heat-1.

Based on the SEM observation, it can be concluded that reaction time also affects the morphology and composition of the inclusions. Elemental analyses of various inclusions in all the specimens have been carried out with an EDS attached with SEM to determine the chemical composition (sulphide/oxide/complex) of inclusions. Presence of oxide

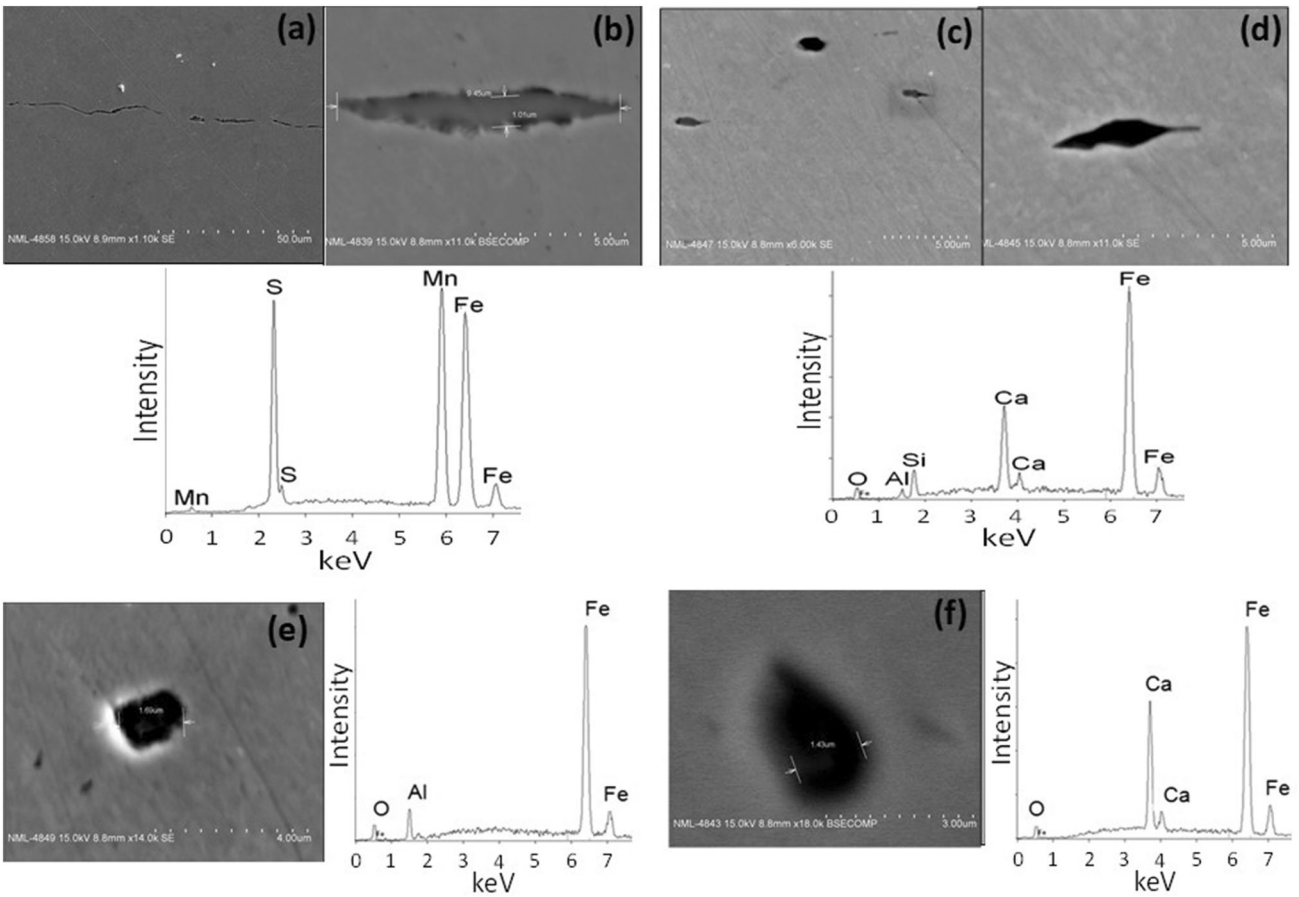

Fig. 9 Elemental analysis of various types of inclusions

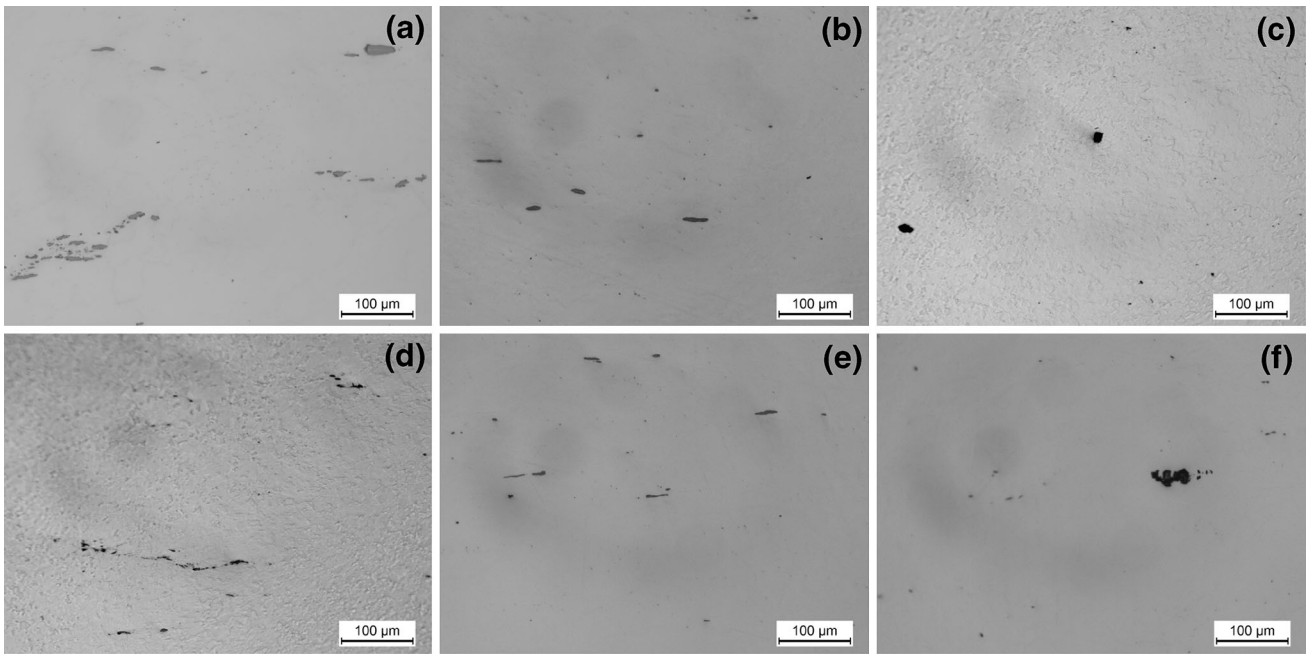

Fig. 10 Optical micrographs of specimens obtained from Heat-1

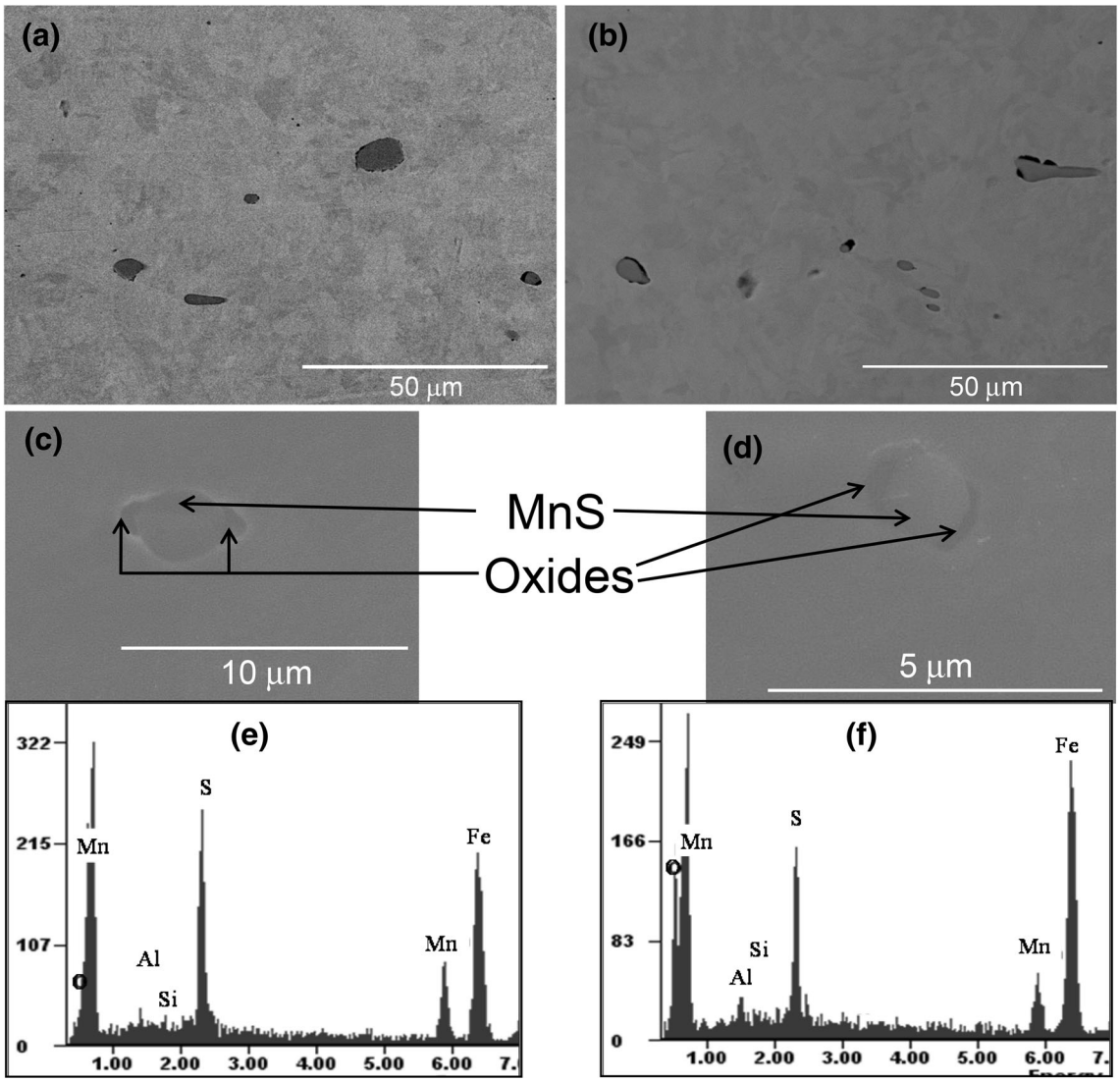

Fig. 11 SEM micrographs showing the presence of mainly MnS inclusions (**a–d**), EDS spot analysis of inclusions (**e–f**)

inclusions is almost negligible for the slag–metal reaction time of 30 min. Oxide inclusions are generally attached to elongated MnS inclusions for the slag–metal reaction time of 15 min. SEM–EDS analysis also confirms the presence of higher amount of MnO in all the oxide inclusions present in Heat-2 in comparison with Heat-1.

Based on the above theoretical and experimental results, it is clearly observed that complex non-deformable oxide inclusions transform to deformable inclusions during top slag treatment of wire rod steels. Bath temperature, refining time, induction rinsing, slag and liquid steel composition and mild vacuum level play a vital role in inclusion transformation. After melting of the wire rod, complex oxides including calcium aluminates and aluminosilicates present in liquid steel are in equilibrium with original composition of liquid steel (refer Figs. 8, 9). After addition of low-basicity synthetic slag with 8% Al_2O_3 into the liquid steel bath, new equilibrium tries to emerge. Manganese and silicon present in liquid steel try to generate new equilibrium with the top slag by forming MnO and SiO_2 to maintain the thermodynamic equilibrium of the system. Simultaneously, inclusions present in liquid steels will also maintain new equilibrium by combining MnO and SiO_2. Therefore, non-deformable high alumina inclusions are converted to low-melting manganese aluminosilicate inclusions. This causes the transformation of $CaO–Al_2O_3/SiO_2–Al_2O_3$-type inclusions to $CaO–Al_2O_3–SiO_2–MnO/SiO_2–Al_2O_3–MnO$-type inclusions. The governing chemical reactions that occur during slag–metal refining are given as follows:

At slag–metal interface,

$$\underline{\mathrm{Mn}} + \underline{\mathrm{O}} \rightarrow (\mathrm{MnO})_{\mathrm{slag}} \quad \text{and} \quad \mathrm{Si} + 2\underline{\mathrm{O}} \rightarrow (\mathrm{SiO_2})_{\mathrm{slag}}$$

At inclusion–liquid steel interface,

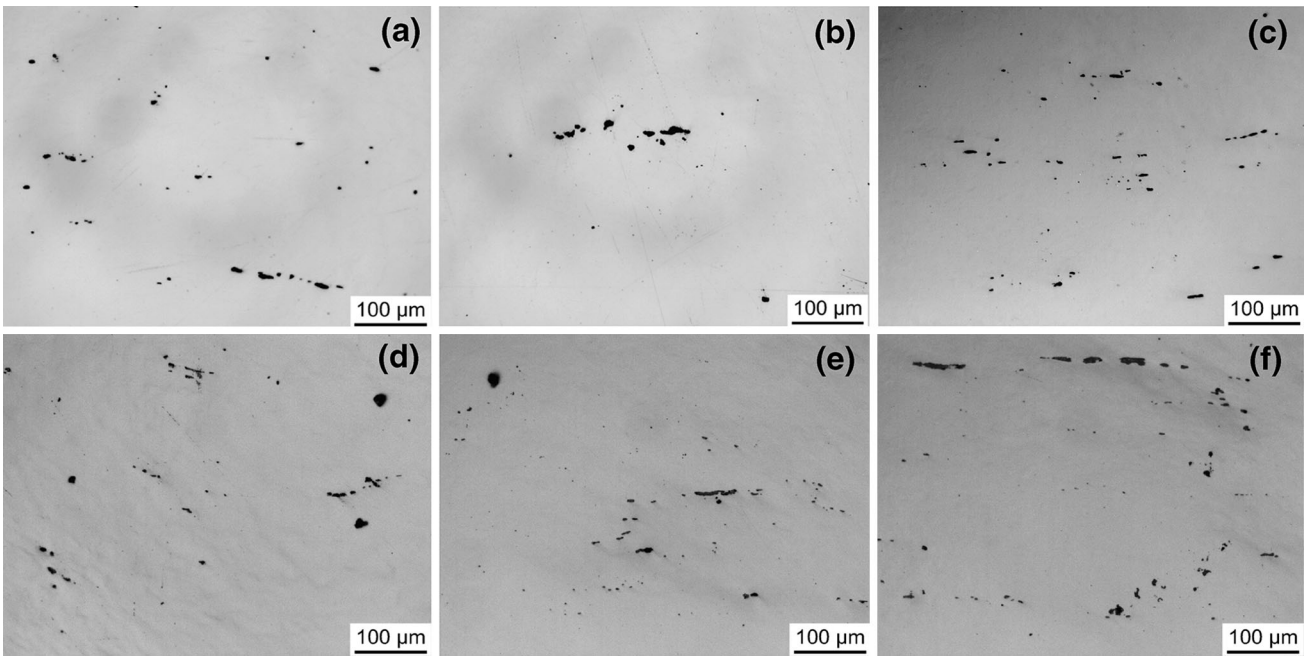

Fig. 12 Optical micrographs of specimens obtained from Heat-2

$$(xCaO \cdot yAl_2O_3)_{inclusion} + z\underline{Si} + z\underline{Mn} + z(3\underline{O}) \rightarrow ((xCaO \cdot yAl_2O_3 \cdot zSiO_2) + zMnO)_{inclusion}$$

$$\Delta G = -2129 + 0.849T \text{ J/mol}$$

$$(xAl_2O_3 \cdot ySiO_2)_{inclusion} + z\underline{Si} + z(2\underline{O}) \rightarrow (xAl_2O_3 \cdot (y+z)SiO_2.)_{inclusion}$$

$$\Delta G = -1096 + 0.517T \text{ J/mol}$$

The complex oxide inclusion $CaO–Al_2O_3–SiO_2–MnO$ type formed due to the above chemical reaction has low melting point ($\approx$ 1450 °C), which floats easily and dissolves in the top slag. Therefore, it can be confirmed that cleanliness of Heat-1 and Heat-2 are improved in comparison with the as-received sample due to the formation of liquid oxide inclusion and followed by absorption of inclusion into the top slag. Near globular inclusions in Heat-2 confirm the presence of SiO_2–Al_2O_3-type oxides, which act as the nucleating site for the precipitation of MnS during solidification (refer Fig. 13). This is attributed to the melting point of aluminosilicates of around 1530 °C, which is higher than the precipitation temperature of MnS. As the treatment time reaches 30 min, complete removal of oxide inclusions takes place and MnS is expected to precipitate during solidification. Very few oxide inclusions observed in Heat-1 are always attached with MnS inclusion. The overall effect of top synthetic slag treatment is to reduce the melting point of non-metallic inclusions, and therefore, transformation of non-deformable to liquid inclusions takes place [9]. This kind of transformation also enhances the floatability of non-metallic inclusions [9]. Designed synthetic slag also has the ability to absorb liquid inclusions such that number of inclusions in the top slag-treated heats are much lesser than as-received wire rod samples (refer Figs. 7, 10, 12).

During top slag treatment of wire rods, stirring of the liquid bath can be controlled by applying mild vacuum, which increases the kinetics of inclusion flotation. The proportion of slag taken for treatment will directly affect compositional changes mainly in terms of Mn and Si in the final steel. 2 wt% slag is added to treat total weight of liquid steel (35 kg), such that final steel composition of wire rod steel after top slag treatment will not change much and it lies well within the industrial requirement. Mild vacuum may also result in minor shifting of thermodynamic equilibrium; however, controlled stirring aids in efficient removal of generated non-metallic inclusion in the intermediate stages of slag–metal reaction and slag composition plays a vital role in absorption of inclusions [9, 22]. The present investigating authors believe that further investigation with the same synthetic slag composition is required for validating the laboratory-scale observation with industry level.

High-carbon wire rod steels are generally produced by Si–Mn killing procedure. Any trace level of aluminium that can come from ferro alloys or refractory or any other sources will increase the dissolved aluminium level in the liquid steel bath. If the dissolved aluminium content in the liquid steel increases beyond 2 ppm, it causes precipitation of alumina or alumina-rich complex inclusions, which are highly detrimental to the wire rod applications. Therefore,

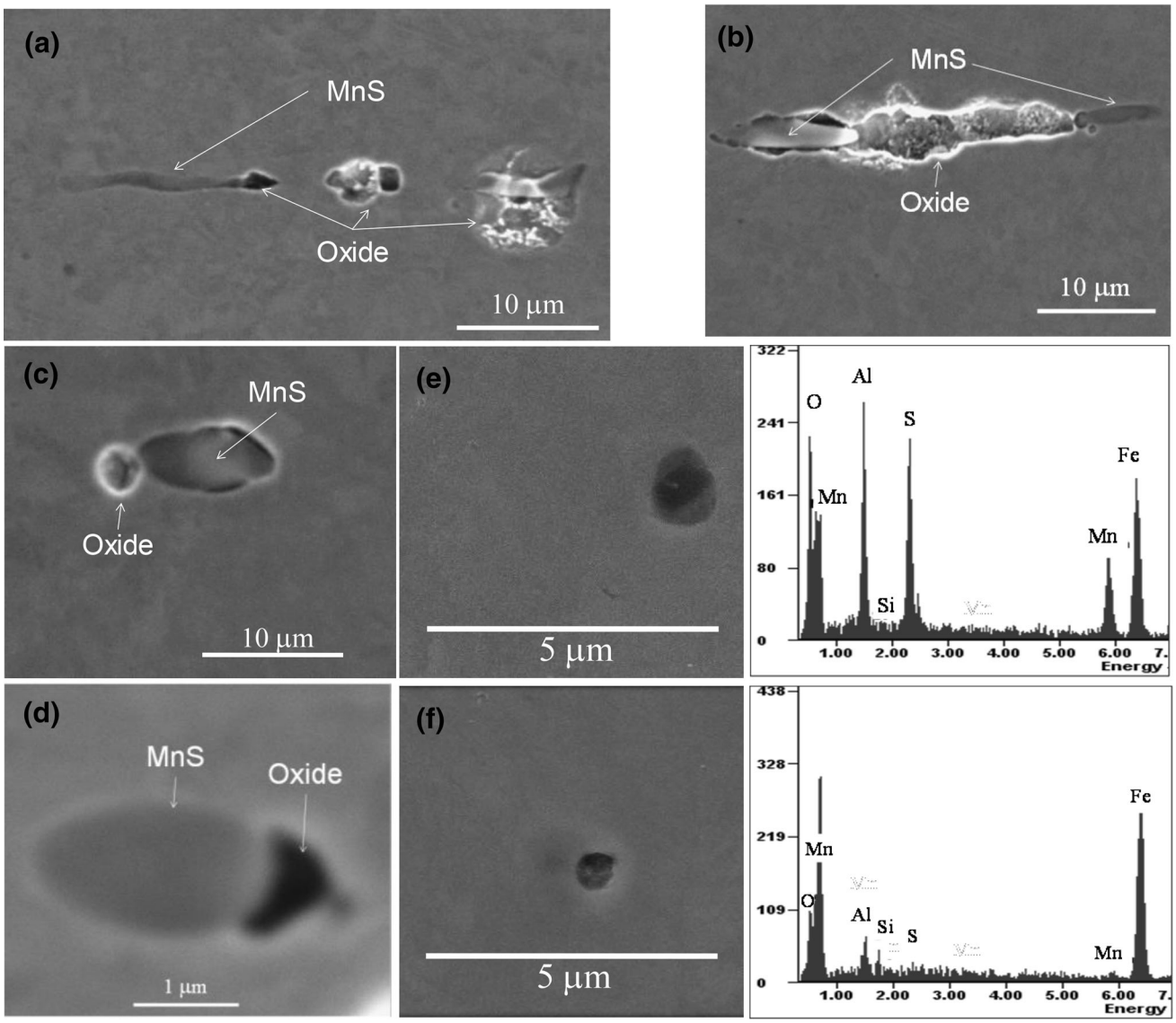

Fig. 13 **a–d** SEM micrograph showing the presence of MnS and oxide inclusions, **e** EDS spot analysis of oxy-sulphide inclusions, **f** EDS spot analysis of oxide inclusion

top slag treatment is one of the commonly employed techniques in steel industries to produce clean wire rod steels. Non-metallic inclusions can be controlled to desired size, shape, distribution and morphology using a top slag of basicity around 1. The present investigation highlights the modification of non-deformable calcium aluminates and calcium aluminosilicates to liquid inclusion by treating the liquid steel with low-basicity top slag. In consequence of this, high-melting aluminosilicates precipitated at high temperature acts as nucleating agent for fine precipitation of MnS during solidification. Based on the understanding developed from this investigation, it is suggested to add the synthetic slag at the beginning of the LF process, such that a minimum slag–metal refining time of 30 min is ensured for successful inclusion transformation and floatation.

5 Summary and Conclusion

The paper discussed both the experimental and theoretical investigations pertaining to control the inclusions in high-carbon wire rods suitable for making wires especially for tire cord applications. It showed the results on the development of synthetic slags with appropriate composition to control the inclusions in the high-carbon wire rods. The results are summarized as follows:

- Synthetic slags having low basicity (CaO/SiO_2 = 0.9–1.2) and low Al_2O_3 content (max 10%) can control the harmful inclusions for the development of special grade high-carbon wires mainly for tire cord applications.

- Synthetic slag having compositions $CaO/SiO_2 = 1$ with Al_2O_3 about 8% is found suitable for controlling inclusions.
- Significant improvement in inclusion rating of hot-rolled specimens prepared by induction melting is obtained by maintaining the residence time of about 30 min across the slag–metal reaction.
- Slag–metal reaction time of 15 min is not sufficient for much improvement in inclusion rating by using these slags.
- Reaction time also affects the morphology and composition of inclusions.

Acknowledgements Authors are thankful to Tata Steel Limited, Jamshedpur, for financial support to carry out this research activity. Authors are also thankful to Dr. S. Prakash, Former Advisor Management, CSIR-NML, and all other project team members for their valuable suggestions and support to execute this work.

References

1. Jung I H, *Comput Coupling Phase Diagr Thermochem* **34** (2010) 332.
2. Zhang L, and Thomas B G, *Metall Mater Trans B* **37** (2006) 733.
3. Zhang L, and Thomas B G, *ISIJ Int* **43** (2003) 271.
4. Ghosh A, *Secondary Steelmaking: Principles and Applications*, CRC Press, Boka Raton (2000), p 255.
5. Kirihara K, *Kobelco Technol Rev* **30** (2011) 62.
6. Van Vlack L H, *Int Met Rev* **22** (1977) 187.
7. Thornton P A, *J Mater Sci* **6** (1971) 347.
8. Jiang Y, Lei J, Zhang J, Xiong R, Zou F, and Xue Z, *J Surf Eng Mater Adv Technol* **3** (2013) 283.
9. Chen S, Jiang M, He X, and Wang X, *Int J Miner Metall Mater* **19** (2014) 490.
10. Liu Z Z, and Cai K K, *Iron Steel* **35** (2000) 64.
11. Beskow K, Jia J, Lupis C H P, and Sichen D, *Ironmak Steelmak* **29** (2002) 427.
12. Fredriksson H, and Hammar O, *Metall Trans B* **11** (1980) 383.
13. Kundu A L, Gupt K M, and Krishna Rao P, *Metall Trans B* **20** (1989) 581.
14. Tozawa H, Kato Y, Sorimachi K, and Nakanishi T, *ISIJ Int* **39** (1999) 426.
15. Goransson M, and Jonson P G, *ISIJ Int*, **41** (2001) S42.
16. Parusov V V, Derevyanchenko I V, Sychkov A B, Nesterenko A M, Parusov É V, and Zhigarev M A, *Metallurgist* **49** (2005) 439.
17. Zhang L, Thomas B G, Wang X, and Cai K, in 85th Steelmaking Conference Proceedings, Warrendale, PA (2002), p 431.
18. Krajnc L, Klancnik G, Mrvar P, and Medved J, *Mater Technol* **46** (2012) 361.
19. Zhang L, *Steel Res Int*, **77** (2006) 158.
20. Dippenaar R, in Tenth International Ferroalloys Congress Proceedings, Cape Town, South Africa (2004), p 741.
21. Jiantao J, Zhenlin L, and Shufeng Y, *Steelmaking* **1** (2014) 18.
22. Prasad A D, and Sankaranarayanan S R, *J Miner Metall Sect B-Metall* **48** (2012) 37.
23. He X F, Wang X H, Chen S H, Jiang M, Huang F X, and Wang W J, *Ironmak Steelmak* **14** (2014) 676.